Virologica Sinica 38 (2023) 66–74

Contents lists available at ScienceDirect

Virologica Sinica

journal homepage: www.keaipublishing.com/en/journals/virologica-sinica
www.virosin.org

Research Article

Mice 3D testicular organoid system as a novel tool to study Zika virus pathogenesis

Wei Yang [a,b], Chen Zhang [a], Yan-Hua Wu [a], Li-Bo Liu [a], Zi-Da Zhen [a], Dong-Ying Fan [a], Zheng-Ran Song [a], Jia-Tong Chang [a], Pei-Gang Wang [a,*], Jing An [a,c,*]

[a] Department of Microbiology, School of Basic Medical Sciences, Capital Medical University, Beijing, 100069, China
[b] Department of Neurosurgery, Capital Medical University Sanbo Brain Hospital, Beijing, 100093, China
[c] Center of Epilepsy, Beijing Institute for Brain Disorders, Beijing, 100093, China

ARTICLE INFO

Keywords:
Organoid
3D cell culture
Testicular organoid model
Zika virus (ZIKV)

ABSTRACT

Zika virus (ZIKV) poses a serious threat to global public health due to its close relationship with neurological and male reproductive damage. However, deficiency of human testicular samples hinders the in-depth research on ZIKV-induced male reproductive system injury. Organoids are relatively simple *in vitro* models, which could mimic the pathological changes of corresponding organs. In this study, we constructed a 3D testicular organoid model using primary testicular cells from adult BALB/c mice. Similar to the testis, this organoid system has a blood-testis barrier (BTB)-like structure and could synthesize testosterone. ZIKV tropism of testicular cells and ZIKV-induced pathological changes in testicular organoid was also similar to that in mammalian testis. Therefore, our results provide a simple and reproducible *in vitro* testicular model for the investigations of ZIKV-induced testicular injury.

1. Introduction

Zika virus (ZIKV) has spread to nearly 100 countries and territories resulting in millions of cases around the world (Gyawali et al., 2016; Xu et al., 2019; Yu et al., 2017), and was announced by the World Health Organization (WHO) as the fourth “public health emergency of international concern (PHEIC)" in 2016 (Lessler et al., 2016). Though clinical symptoms of ZIKV patients are mainly mild and self-limiting (Pielnaa et al., 2020), ZIKV is still an international concern due to its link with Guillain-Barre syndrome and microcephaly (Cao-Lormeau et al., 2016), along with the potential threat to the male reproductive system (Li et al., 2018; Liu et al., 2018; Pielnaa et al., 2020; Shan et al., 2018). More importantly, some ZIKV male patients showed reproductive system symptoms including prostatitis, hemospermia and increased leukocyte count in semen (Foy et al., 2011; Kurscheidt et al., 2019; Torres et al., 2016). Testosterone values of ZIKV-infected men also show a trend toward lower values at day 7 after symptom onset (Joguet et al., 2017). The direct evidence of ZIKV-induced male fertility deficiency is that the sperm counts of 15 male volunteers with acute ZIKV infection were significantly reduced from a median 119 $\times$ 10^6 spermatozoa at day 7–45.2 $\times$ 10^6 at day 30 (Joguet et al., 2017).

At present, a variety of animal models, including genetically modified mice (interferon receptor gene knockout mice and hSTAT2 knock-in mice, etc.), interferon receptor blocking antibodies-injected mice and nonhuman primates, have been used to explore the mechanism of ZIKV-induced male reproductive system damage, and the testis has been proved to be the main targets of ZIKV, as most testicular cells were susceptible to ZIKV (Coffey et al., 2017; Yang et al., 2020; Dudley et al., 2016; Strange et al., 2019; Gorman et al., 2018; Kumar et al., 2018; Govero et al., 2016; Haddow et al., 2017; Hirsch et al., 2017; Ma et al., 2016; Osuna et al., 2016; Pardi et al., 2017; Richner et al., 2017; Sheng et al., 2017). However, these animal models still have room for improvement. Gene modification strategy of immune deficient mice resulted in a more severe testicular pathological change than ZIKV male patients. Nonhuman primates are extremely expensive, thus can't be wildly used, and human testicular tissues are difficult to obtain.

Organoids are *in vitro* constructs obtained from embryonic stem cells (ESCs), induced pluripotent stem cells (iPSCs) or adult stem cells (ASCs) (Driehuis et al., 2020a). With three dimensional (3D)-cell culture technology, variety of cells “self assemble” by their cell polarity to form cell clusters with specific spatial structure, so as to mimic organ formation and physiological structure (Clevers, 2016; Lancaster and Knoblich,

* Corresponding authors.
E-mail addresses: pgwang@ccmu.edu.cn (P.-G. Wang), anjing@ccmu.edu.cn, 15810200117@163.com (J. An).

https://doi.org/10.1016/j.virs.2022.10.001
Received 27 May 2022; Accepted 8 October 2022
Available online 12 October 2022

2014). Many kinds of organoid systems are now applied as *in vitro* model of viral infection, such as intestinal organs for norovirus (Ettayebi et al., 2016), human bronchial organs for avian influenza and swine influenza (Zhou et al., 2018), and brain organoids for the investigation of ZIKV infection in brain tissues (Garcez et al., 2016; Qian et al., 2016). These organoids reduce the use of animals and provide convenient tools for viral study. For ZIKV-induced injury, although researchers have conducted in-depth research on the central nervous system damage, due to the lack of human testicular samples, the mechanism underlying ZIKV-induced male reproductive system injury is still unclear. Therefore, it is urgent to develop a convenient and accessible research model that can mimic the pathological characteristics of ZIKV-infected testicular tissue.

In this study, we constructed a mice 3D testicular organoid system by planting primary testicular cells from adult BALB/c mice in a 3D culture microplate. The testicular organoid system has similar physiological structure and function to mammalian testis, and is thus feasible in the investigation of ZIKV-induced testicular damage.

2. Material and methods

2.1. Virus

Asian ZIKV (strain SMGC-1, GenBank accession number: KX266255) was propagated in C6/36 cells and the titer was determined by plaque assay on Vero cell with 1.0% methylcellulose. Virus was stored at −80 °C until use.

2.2. Mouse experiments

SPF BALB/c mice were purchased from Charles River company (Beijing) by the Animal Department of Capital Medical University, and bred under specific pathogen-free conditions at Capital Medical University. 6–8 weeks old male BALB/c mouse were euthanized by cervical dislocation, testes were then harvested and immediately fixed in Modified Davidson's Fluid solution (30 mL of 40% formaldehyde, 15 mL of ethanol, 5 mL of glacial acetic acid and 50 mL of distilled water) overnight, then dehydrated and paraffin-embedded.

2.3. Preparation of testicular organoids

Preparation of testicular organoids was carried out with reference to the previous research (Sakib et al., 2019), and the protocol is as follows:

2.3.1. Isolation of mice primary testicular cells

(1) Testicular tissue was collected from 6–8-week-old male BALB/c mice and cut to about 2 mm × 2 mm × 2 mm. Subsequently, testicular tissue was digested with Hank's balanced salt solution (HBSS, GIBCO) containing type IV collagenase (2 mg/mL) at 37 °C for 15 min. After centrifugation at 90×*g* for 1.5 min, the seminiferous tubules were washed with HBSS;
(2) The seminiferous tubules were digested with 0.25% trypsin EDTA containing DNase I (7 mg/mL) to isolate single testicular cells and obtain testicular single cell suspension. All experiments were repeated with at least three independently cell suspensions.

2.3.2. Generation of three-dimensional (3D) testicular organoids in microporous culture plate

(1) Pretreatment of Aggrewell 400 plate (stemcell Technologies Inc, Vancouver, Canada, cat#34450): the plate was washed once with 0.5 mL/well PBS, then organoids formation medium was added (Dulbecco Modified Eagle Medium F/12 supplemented with insulin 10 μg/mL, transferrin 5.5 μg/mL, selenium 6.7 ng/mL, 20 ng/mL epidermal growth factor, 1% Penicillin-Streptomycin) to the plate at 0.5 mL/well. Plates were centrifugated at 2000×*g* for 2 min to remove the trapped air;
(2) Each well contained 1.2×10^6 (for 1000 organoids) or 6×10^5 (for 500 organoids) testicular cells in 0.5 mL organic matter forming medium. Culture medium for mouse samples was supplemented with 1:100 dilution of Matrigel (MATRIGEL MATRIX 5 ML, T_701CB-40234, Thermo Fisher Scientific). Plate was then centrifugated at 500 ×*g* for 5 min;
(3) The microplate was continuously cultured in 37 °C with 5% CO_2 for 7 days. The medium of organoids was half changed every other day. The organoids were photographed under the light microscope every day.

2.4. Collection of testicular organoid samples

(1) Testicular organoids infection experiment: the culture medium was aspirated away and the plate was washed with HBSS for 3 times. 1×10^5 PFU/well ZIKV was added, and the virus and testicular organoids were incubated at 37 °C and 5% CO_2 for 1 h. Subsequently, the virus solution was aspirated away. After 3 times of washing with HBSS, 1 mL/well organic substance containing matrix gel was added into the plate, and the testicular organoids were incubated at 37 °C and 5% CO_2 for sampling;
(2) Preparation of testicular organoids smears: the culture medium was aspirated away and the plate was washed with HBSS for 3 times. Subsequently, testicular organoids were fixed with 4% paraformaldehyde for 15 min. After the paraformaldehyde solution was aspirated away, 0.5 mL/well HBSS was added into the plate, then the plate was gently blew to harvest testicular organoids suspension. Then 100 μL testicular organ suspension was added onto a clean glass slide to make a smear, then the testicular organ was dried at room temperature for 5–10 min, and was stored at −30 °C;
(3) Collection of testicular organoids RNA: the culture medium was aspirated away and the plate was washed with HBSS for 3 times. Then transzol was added with 0.5 mL/well (TransGen Biotech), and the liquid was blew to suspend the testicular organoids, then the total RNA was extracted according to the instructions;
(4) Collection of testicular organoids culture medium: the culture medium was collected in half exchange solution during the formation of testicular organoids or after ZIKV infection, and stored at −80 °C. The total RNA in the culture medium was extracted by transzol (TransGen Biotech).

2.5. Hematoxylin and eosin (H&E) analyses

Testes embedded in paraffin were sectioned (5 μm in thickness) and testicular sections were then subjected to H&E staining. Sections were immersed in xylene and alcohol, then stained with hematoxylin for 12 min. After stained with eosin for 20 min and re-immersed in alcohol and xylene, sections were mounted using synthetic resin.

2.6. Immunofluorescence staining (IFA)

Testes sections or testicular organoids smears were incubated with the following primary antibodies overnight at 4 °C, including rabbit anti-mouse claudin-1 (CLDN1) (1:200, Abcam, ab15098), rabbit anti-mouse occludin (OCLN) (1:200, Abcam, ab167161), rabbit anti-mouse zonula occluden-1 (ZO-1) (1:200, Thermo Fisher, 33–9100), rabbit anti-mouse caspase-9 (1:500, Abcam, ab202068), rabbit anti-mouse cleaved caspase-3 (1:500, Cell Signaling Technology, 9664S), mouse anti-DDX4 (1:100, Abcam, ab27591), rabbit anti-mouse DDX4 (1:100, Abcam, ab13840), mouse anti-mouse Vimentin (1:100, Abcam, ab8978), rabbit anti-mouse α-SMA (1:100, Abcam, ab5694), rabbit anti-mouse HSD3B1 (1:100, Abcam, ab65156), rat anti-mouse C3 (1:100, Abcam, ab11862), rabbit anti-mouse membrane attack complex (MAC) (1:100, Abcam,

ab55811) or mouse anti-ZIKV antibody 4G2 (1:500). After washed with PBS, sections were incubated with secondary antibodies at 37 °C for 1 h in the dark conditions, including donkey anti-mouse IgG (1:1000, Alexa Fluor R 488, A21202, Life technologies), donkey anti-rabbit IgG (1:1000, Alexa Fluor R 594, A21207, Life technologies). Images were captured with Olympus microscope (IX71, Olympus, Japan).

2.7. ZIKV mRNA quantification

ZIKV-infected and control mice were euthanized, and blood and testes were harvested at different time points as indicated. Samples were homogenated in TransZol (TransGen China, ET101-01) and RNA was extracted according to manufacturer protocol. Real-time qPCR analyses were performed as previously reported (Sheng et al., 2017) with Quant One Step qRT-PCR (Tiangen, China) on 7500 Real Time PCR System (Applied Biosystems, USA). Quantification of the copies of ZIKV mRNA was determined using the standard curve method. ZIKV genome RNA transcribed *in vitro* was quantified and used as a standard template to establish the standard curve. The primer sequences were as follows: forward: 5′-TCAGACTGCGACAGTTCGAGT-3′; reverse: 5′-GCATATTGA CAATCCGGAAT-3′.

2.8. ELISA

Concentrations of testosterone in supernatant of testicular organoids were quantified by ELISA according to the manufacturer's instructions. Testosterone reagents were purchased from Cloud-Clone (CEA458Ge, Cloud-Clone, China). Briefly, 100 μL standard or testis tissue supernates (100 μL/well) was added, then plate was incubated for 1 h at 37 °C. Subsequently, 50 μL Detection Reagent A was added and the plate was incubated for 1 h at 37 °C. After washing, 50 μL Detection Reagent B was added and incubated for 30 min. Finally, 90 μL Substrate Solution was added and incubated at 37 °C for 15 min, followed by addition of 50 μL Stop Solution. The absorbance was measured at 450 nm in a Multiskan spectrum 1500 (Thermo, USA).

2.9. Western blotting

Relative expression of tight junction proteins of ZIKV-infected and uninfected testicular organoids was measured by Western blot. Organoids at 3 days post infection (dpi) were harvested and lysed by radioimmunoprecipitation assay (RIPA) lysis buffer containing protease inhibitor. After determination of protein concentration in each sample by BCA Protein Assay kit (Thermo Fisher Scientific, Waltham, Massachusetts, USA), samples were subjected to 10% sodium dodecyl sulfate polyacrylamide gel electrophoresis and transferred onto polyvinylidene difluoride (PVDF) membranes. Membranes were blocked in 5% milk at room temperature for 1 h, then incubated with rabbit anti-mouse ZO-1 (1:200, Thermo Fisher, 33–9100), rabbit anti-mouse CLDN1 (1:200, Abcam, ab15098), rabbit anti-mouse occludin (1:200, Abcam, ab167161) or rabbit anti-β-actin mAb (1:1000, Cell Signaling Technology, 4970S) antibodies separately at 4 °C overnight. After incubation with peroxidase-linked secondary antibodies, membranes were subjected to an Odyssey infrared imaging system (Odyssey LI-COR Biosciences, Lincoln) to visualize the protein expression.

2.10. Statistical analysis

SPSS 17.0 Software (IBM, Armonk, NY, USA) was used for statistical analysis. The quantitative data between two groups with normal distributions was analyzed using the repeated-measures analysis of variance or the Student's *t*-test. All results were presented as the mean ± standard error of the mean (SEM) in this research from at least three different repeats. $P < 0.05$ was considered as statistically significant between two groups.

3. Results

3.1. Formation of the mice 3D testicular organoid system

Primary testicular cells collected from 6–8-week-old male BALB/c mice were cultured in AggreWell 400 plate to construct testicular organoids. To determine the morphology of testicular organoids, we first photographed testicular organoids during 0–7 days post culture. Primary testicular cells accumulated in the chambers of microplate at 0–2 days. During 3–6 days post culture, testicular cells gradually accumulated tightly and assembled into cell clusters. At the 7th day post culture, testicular cells completely gathered into oval, dense cell clusters with smooth boundaries and about 20–30 μm in diameter (Fig. 1A).

Secondly, the distribution of various testicular cells in organoid system was detected by immunofluorescence staining (IFA), and the location of spermatogenic cells (DDX4+), Sertoli cells (Vimentin+), myoid epithelial cells (α-SMA+) and Leydig cells (HSD3B1+) in testicular organoids was compared with testis from adult BALB/c mice. In testicular organoids at the 5th day post culture, DDX4+ spermatogenic cells did not converge into tight cell cluster, and the rest of testicular cells were scattered around spermatogenic cells at outer layer (Fig. 1B–D). While in the shaped testicular organoids at the 7th day post culture, a dense cell cluster composed of DDX4+ spermatogenic cells were arranged in center of testicular organoids surrounded by consecutively arranged Vimentin + Sertoli cells at outer layer (Fig. 1B), α-SMA + myoid epithelial cells and HSD3B1+ Leydig cells were also mainly arranged at the outer layer (Fig. 1C and D). H&E staining of testes from BALB/c mice showed that spermatogenic cells are encapsulated by Sertoli cells and myoid epithelial cells in seminiferous tubules (Fig. 1E).

The above results showed that the structure of testicular organoid was similar to that of seminiferous tubule of adult BALB/c mice, indicating that the morphology of testicular organoid system was consistent with the basic structure of the testis.

3.2. Physiological function of mice 3D testicular organoids

The blood-testis barrier (BTB) is an important barrier structure of the testis, which is constituted by specialized junctions between adjacent Sertoli cells near the basement membrane (Dym, 1994; Siu and Cheng, 2004, 2008). BTB protects spermatogenic cells from immune attack and pathogen invasion by separating spermatogenic cells in the tubule lumen from immune cells in the interstitial space. In order to evaluate the barrier structure of 3D testicular organoids, we detected the expression and distribution of tight junction proteins ZO-1, OCLN and CLDN-1 in shaped testicular organoids by IFA, and compared with testes from adult BALB/c mice. At the 5th day post culture, tight junction proteins were distributed discontinuously at the outer layer of organoids in testicular organoids (Fig. 2A). At the 7th day post culture, ZO-1 and CLDN-1 were distributed in a continuous strip shape at the outer layer, while OCLN extended radially along the outer layer to the inner part of testicular organoids (Fig. 2A). In adult mouse testes, ZO-1 was mainly distributed at the basement membrane of seminiferous tubules, around the boundary of Sertoli cells, while OCLN extended radially to the lumen along the boundary of Sertoli cells, and some of them were wrapped with spermatogenic cells. CLDN-1 was arranged in a cord shape around Sertoli cells, and was also located on the luminal surface of spermatogenic cells (Fig. 2B). The staining results showed that these 3D testicular organoids had a BTB structure similar to that of mouse testes.

Testosterone synthesis is one of the most important physiological functions of mammalian testes. Testosterone plays an important role in maintaining male secondary sexual characteristics and fertility (Gagliano-Juca and Basaria, 2019). To further evaluate the physiological function of the organoid system, we next detected its testosterone synthesis ability by ELISA. Testosterone concentration in testicular organoid culture medium gradually increased at 2–4 days post culture, then peaked and remained stable at 6–8 days post culture (Fig. 2C), suggesting that

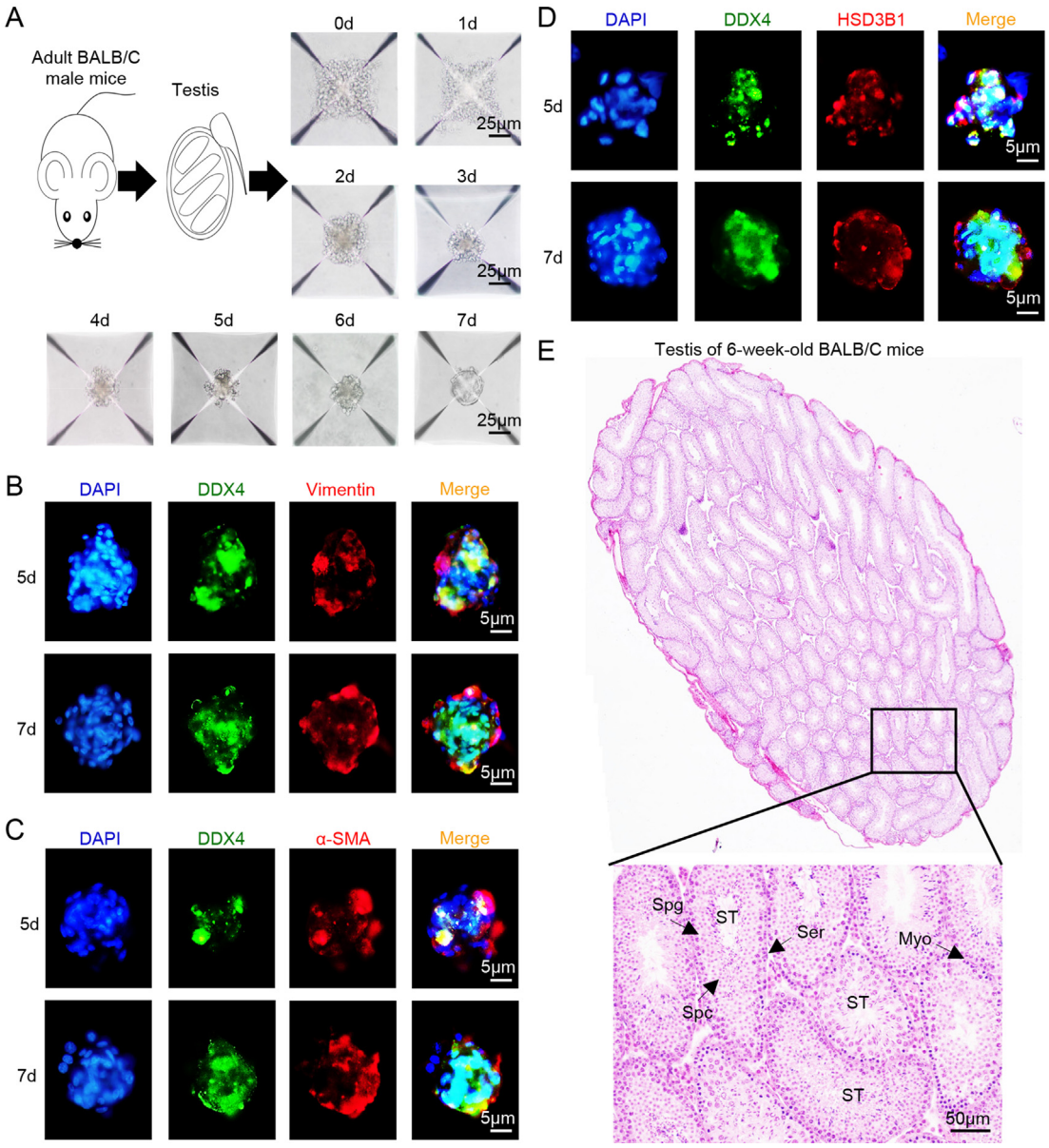

Fig. 1. Arrangement of testicular cells in mice 3D testicular organoids. **A** The morphological structure of testicular organoids at 0–7 days post culture. Scale bar = 25 μm. **B–D** Distribution of spermatogenic cells marker DDX4 and Sertoli cells marker Vimentin (**B**), myoid epithelial cells marker α-SMA (**C**) or Leydig cells marker HSD3B1 (**D**) in shaped testicular organoids at 5th and 7th day post culture. Nuclei were visualized with DAPI. Scale bar, 5 μm. **E** H&E staining of the testis from 6 to 8 weeks old BALB/c male mice (ST: seminiferous tubule, Spg: spermatogonia, Spc: spermatocytes; Ser: Sertoli cell; Myo: myoid epithelial cell). Scale bar, 50 μm.

the synthesize of testosterone gradually enhanced as the formation of testicular organoids.

In conclusion, these results showed that this testicular organoid system had a BTB-like barrier structure and testosterone synthesis ability similar to the testis, thus could be used as an *in vitro* testis culture model.

3.3. Evaluation of the susceptibility of testicular organoids to ZIKV

Testes are the main target organs of ZIKV in male reproductive system. We further analyzed the feasibility of this organoid system as a ZIKV infection model by evaluating its susceptibility to ZIKV. After infected with 1×10^5 PFU ZIKV at the 7th day post culture, the morphology of testicular organoids was photographed, and no significant changes in organoid morphology at 0–3 dpi was found when compared with the uninfected controls (Fig. 3A).

The distribution of ZIKV antigens in testicular organoids were also detected by IFA. ZIKV antigens mainly distributed in the outer layer of testicular organoids at 1 dpi, and there was no co-stained signal with spermatogenic cell marker DDX4. At 3 dpi, a small amount of ZIKV antigens was detected in the interior of testicular organoids, and co-located with DDX4 (Fig. 3B). The distribution of ZIKV antigens in testicular organoids was consistent with those of testicular cells infected by ZIKV reported by current studies (Mlera and Bloom, 2019; Robinson et al., 2018; Sheng et al., 2017), suggesting that ZIKV tropism of testicular cells in this organoid system was similar to that in testes.

The replication of viral RNA in ZIKV-infected testicular organoids was also detected by RT-qPCR. It showed that ZIKV viral load in testicular organoids was gradually increased during 1–3 dpi (Fig. 3C). In addition, viral load in the organoid culture medium was also detected, and in line with results in testicular organoids, viral load in the culture medium was

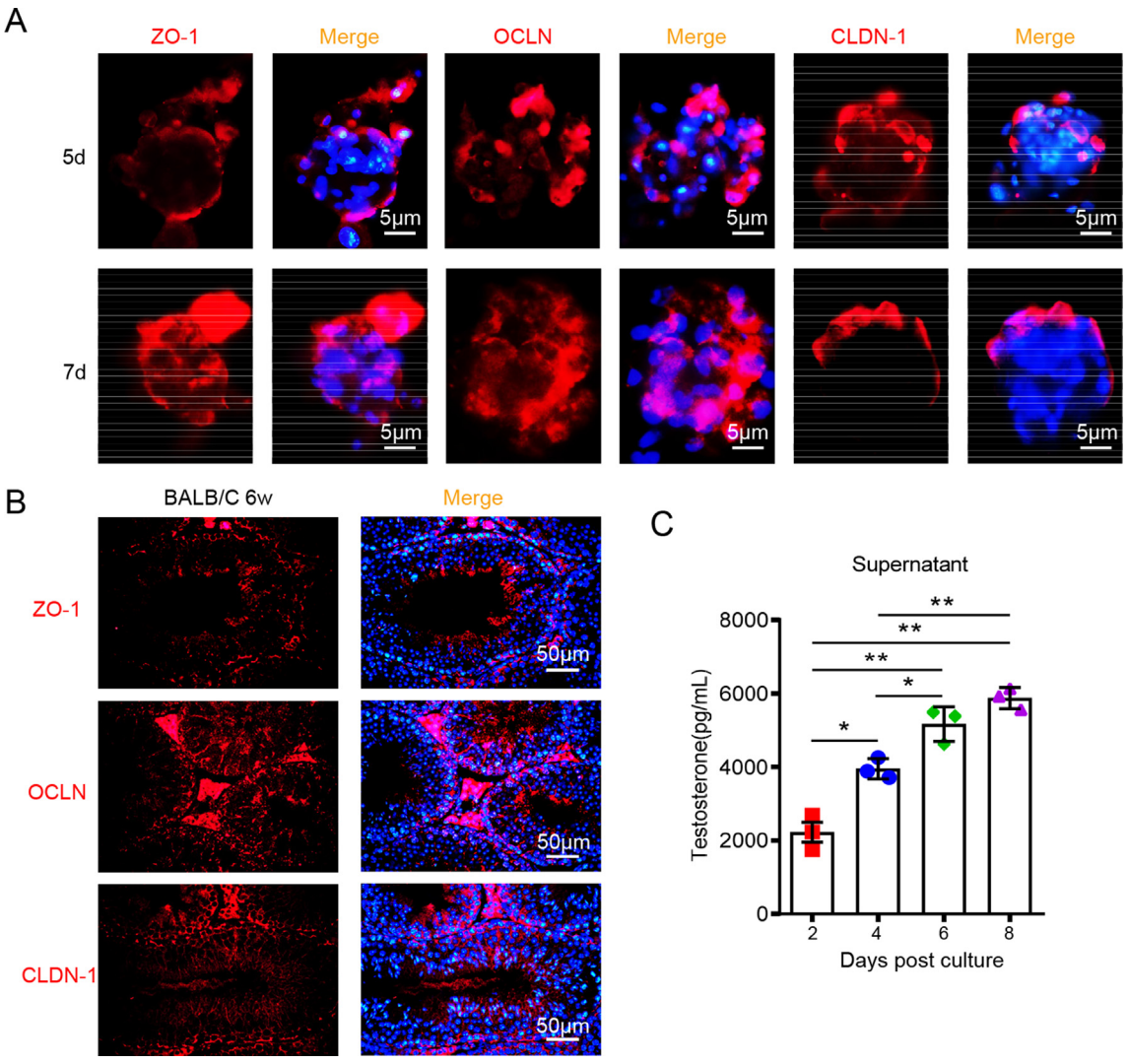

Fig. 2. Mice 3D testicular organoids have BTB structure and physiological function similar to mice testis. **A** Distribution of ZO-1, OCLN or CLDN-1 in testicular organoids at the 5th and 7th day post culture. Nuclei were visualized with DAPI. Scale bar, 5 μm. ZO-1: zonula occluden-1; OCLN: occludin; CLDN-1: claudin-1. **B** Distribution of ZO-1, OCLN or CLDN-1 in the testis from 6 to 8 weeks old BALB/c male mice. Nuclei were visualized with DAPI. Scale bar, 50 μm. **C** The concentration of testosterone in organoid cultured medium at 2–8 days post culture was analyzed by ELISA (n = 500 testicular organoids/data point, $*P < 0.05$, $**P < 0.01$).

also significantly increased from 1 to 3 dpi (Fig. 3D). The results above showed that these testicular organoids were susceptible to ZIKV infection and could support the replication and release of ZIKV. Therefore, this organoid system was a testis-like model which could be used to investigate the mechanism of ZIKV-induced testicular injury.

3.4. *Effect of ZIKV infection on testicular organoids*

We have demonstrated that the susceptibility of testicular cells in testicular organoids to ZIKV was consistent with the results in current studies. In this section, we further evaluated the effect of ZIKV on testicular organoids by IFA. Tight junction proteins such as ZO-1, OCLN and CLDN-1, was reported to be decreasingly expressed during ZIKV infection (Mlera and Bloom, 2019; Robinson et al., 2018; Sheng et al., 2017). At 1–3 dpi, it was detected that the expression of ZO-1, OCLN and CLDN-1 was slightly decreased (Fig. 4A). Western blot assay also showed a decreasing trend of the expression of tight junction proteins after infection (Fig. 4B). Thus, ZIKV infection may destroy the BTB-like structure of organoids. ELISA also showed that the testosterone concentration in testicular organoid culture medium significantly decreased at 1–3 dpi (Fig. 4C), suggesting that ZIKV infection could also repress testosterone synthesis. These results were consistent with the results of ZIKV-induced testicular injury in animal models (Govero et al., 2016; Ma et al., 2017), indicating that ZIKV infection will not only destroy the barrier structure of testicular organoid, but also repress the testosterone synthesis. The mechanism of ZIKV-induced testicular injury is one of the main focuses in ZIKV research. In order to explore the effect of ZIKV infection on the survival of testicular cells, we detected the expression of apoptosis markers in ZIKV-infected testicular organoids by IFA. Compared with uninfected testicular organoids, expression of endogenous apoptosis marker caspase-9 and apoptosis terminal marker cleaved caspase-3 did not increase at 3 dpi (Fig. 4D and E).

The above results suggested that ZIKV infection could destroy barrier structure and repress the testosterone synthesis of testicular organoids, although similar to symptoms in male patients and animal models, it is not the main factor leading to the injury of testicular cells. The testicular organoids provide a useful tool for the investigation of the mechanism of ZIKV-induced testicular injury.

4. Discussion

Since its epidemic in 2015, ZIKV has infected millions of people around the world (Ferraris et al., 2019). Although researchers have revealed the specific mechanism of ZIKV-induced microcephaly (Faizan et al., 2016; Li et al., 2016), the pathogenesis of ZIKV-induced male

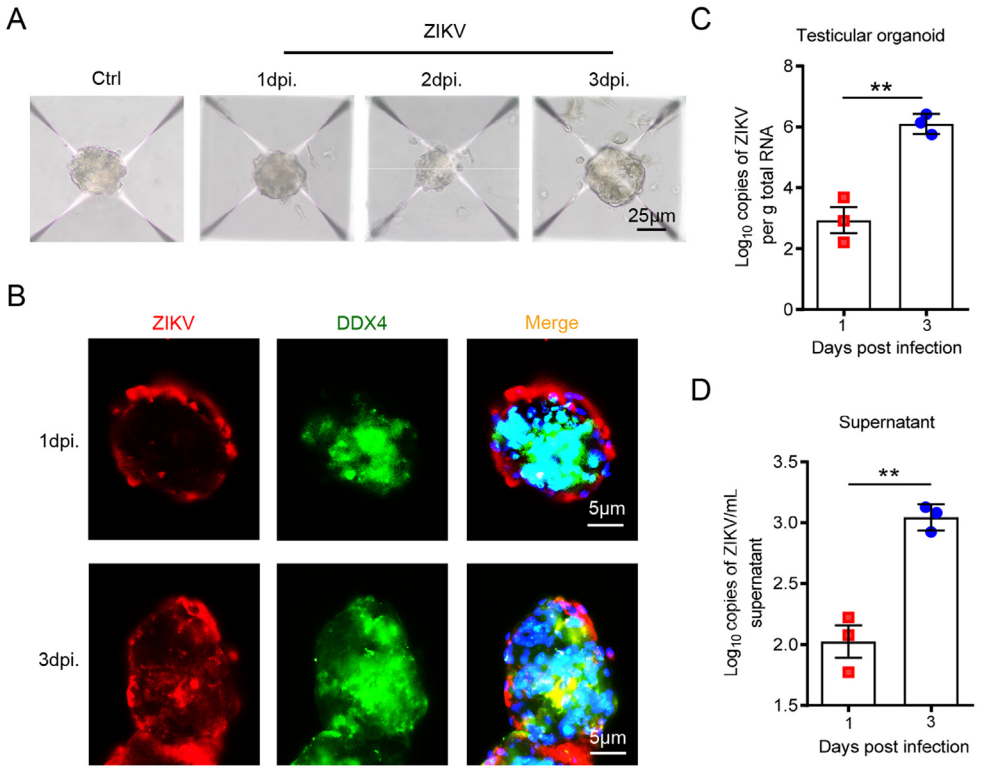

Fig. 3. Mice 3D testicular organoids can support ZIKV infection and replication. **A** The morphological structure of testicular organoids at 1–3 dpi. Scale bar = 25 μm. **B** Distribution of ZIKV antigens and spermatogenic cell marker DDX4 in testicular organoids at 1–3 dpi. Nuclei were visualized with DAPI. Scale bar, 5 μm. **C** & **D** ZIKV viral load in testicular organoids (**C**) or organoid cultured medium (**D**) at 1–3 dpi was analyzed by RT-qPCR, $^{**}P < 0.01$.

reproductive system injury is still unclear. In this study, we constructed a 3D testicular organoid system by using primary testicular cells from adult BALB/c mice which could simulate the physiological structure and function of mammalian testis. *In vitro* infection experiments indicated that although the cell tropism of ZIKV and ZIKV-induced structural and functional damage in organoid system were consistent with the existing researches (Faizan et al., 2016; Li et al., 2016), ZIKV infection was not the main factor leading to the damage of testicular cells. In conclusion, we constructed a replicable testicular organoid system which could mimic most of ZIKV-induced pathological features in mammalian testicular cells. Therefore, this testicular organoid system was a reasonable and promising *in vitro* ZIKV infection research model.

Testes were the main target organs of ZIKV infection in male reproductive system (Halabi et al., 2020; Ma et al., 2016; Pletnev et al., 2021), and various animal models have been used to investigate ZIKV-induced testicular injury. However, most murine models cannot simulate all the symptoms of ZIKV patients (Pletnev et al., 2021; Richner et al., 2017), and non-human primate models are not suitable for large-scale experiments (Dudley et al., 2016; Osuna et al., 2016). Thus, it is still urgent to develop a model which can mimic ZIKV-induced human testicular pathological characteristics. Organoid is a construct obtained by *in vitro* culture of embryonic stem cells (ESCs), induced pluripotent stem cells (iPSCs) or adult stem cells (ASCs) (Driehuis et al., 2020b). Through the difference of cell polarity, organoids can form micro spheres with specific cell composition and spatial structure, so as to mimic the physiological or pathological state of specific organs (Clevers, 2016; Lancaster and Knoblich, 2014). The culture methods of testicular organoids mainly include two strategies: 2D and 3D testicular organoids (Richer et al., 2020). 2D testicular organoids were formed by culturing primary testicular cells or single Sertoli cells *in vitro*, and these organoids showed a linear or sheet structures (Mackay et al., 1999; Tung and Fritz, 1984; van der Wee and Hofmann, 1999; Willerton et al., 2004) (Gassei et al., 2006; Mincheva et al., 2018; Schlatt et al., 1996; von Kopylow et al., 2018). However, limited by the plane structure, BTB structure of 2D organoids is incomplete. 3D testicular organoids were formed by the suspension of testicular cells in matrix gel, which could form a mass structure of spermatogenic cells encapsulated by Sertoli cells and epithelial cells similar to testes (Hadley et al., 1985; Legendre et al., 2010; Zhang et al., 2017). Therefore, 3D testicular organoid system is a more valuable *in vitro* testis model.

In this study, in order to evaluate the structure and function of 3D testicular organoids, we first analyzed the distribution of testicular cells by IFA. Similar to testes from adult BALB/c male mice, Sertoli cells, myoid epithelial cells and Leydig cells mainly located at the outer layer of testicular organoids, while almost all DDX4+ spermatogenic cells located inside the organoids. In addition, the arrangement of tight junction proteins ZO-1, OCLN and CLDN-1 was also consistent with that of mouse testes. In terms of testicular physiological function, testosterone concentration in culture medium was detected by ELISA, and during the formation of testicular organoids, concentration of testosterone gradually increased, suggesting that testicular organoids could synthesize and secret testosterone. This phenomenon also showed that interaction between testicular cells was important for testosterone synthesis, which is also consistent with the androgen synthesis function of testis.

Next, we investigated the susceptibility of 3D testicular organoids to ZIKV infection. In line with the results of previous studies (Matusali et al., 2018; Siemann et al., 2017), Sertoli cells and spermatogenic cells in testicular organoids were susceptible to ZIKV, and viral load in testicular organs and culture medium gradually increased after infection, indicating that these testicular organoids could support the infection and replication of ZIKV. We further detected the expression and distribution of tight junction proteins in ZIKV-infected testicular organoids, and tight junction proteins showed a discontinuous distribution and down-regulated expression level compared with uninfected controls. Consistent with the trend toward lower testosterone values in male patients (Joguet et al., 2017), testosterone synthesis of testicular organoids was also repressed after ZIKV infection as shown by ELISA. These

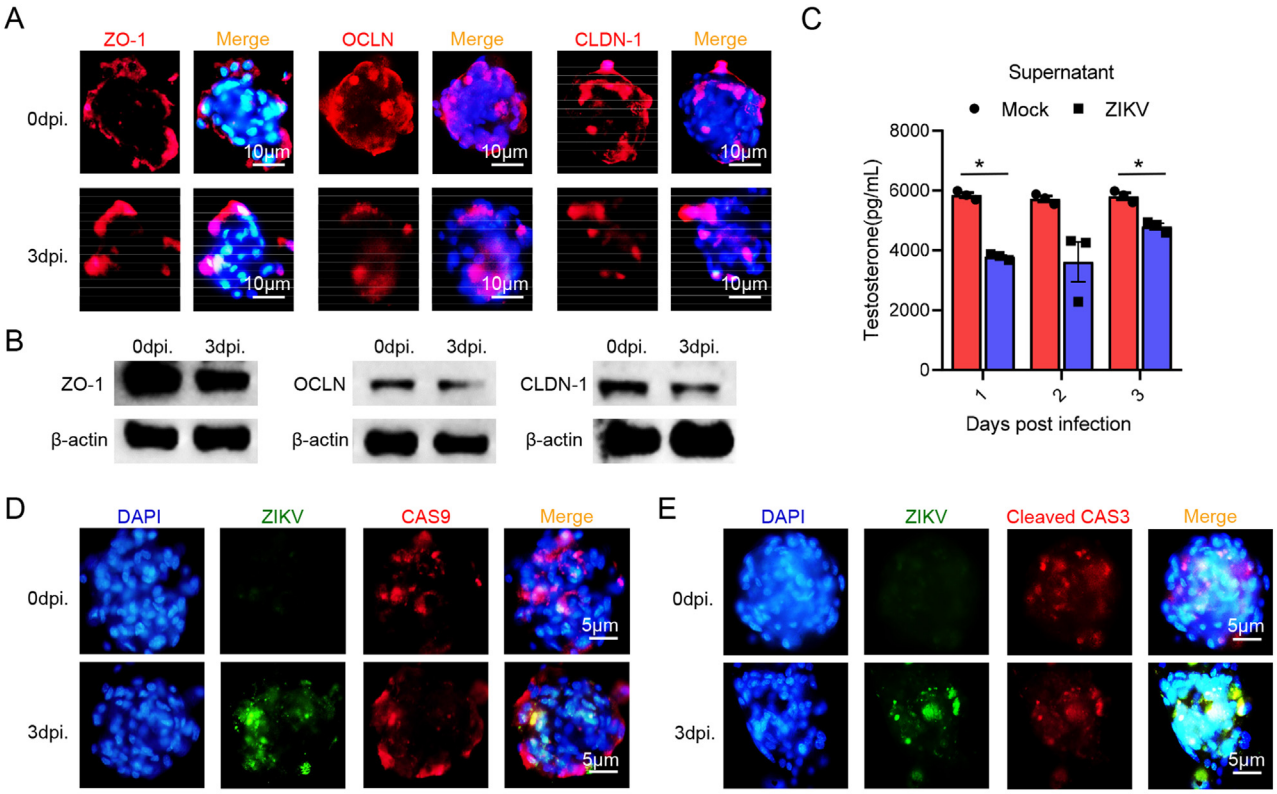

Fig. 4. ZIKV infection damages the barrier structure and physiological function of mice 3D testicular organoids. **A** Distribution of ZO-1, OCLN or CLDN-1 in testicular organoids at 3dpi. Nuclei were visualized with DAPI. Scale bar, 10 μm. ZO-1: zonula occluden-1; OCLN: occludin; CLDN-1: claudin-1. **B** Expressions of ZO-1, OCLN and CLDN-1 in ZIKV-infected testicular organoids as well as their corresponding controls were visualized by Western blot. (n = 1500 testicular organoids/strip). **C** The concentration of testosterone in organoid cultured medium at 1–3 dpi was analyzed by ELISA, medium of uninfected organoids served as Mock (n = 500 testicular organoids/data point, $^{**}P < 0.01$). **D** & **E** Distribution of ZIKV antigens and caspase-9 (**D**) or cleaved caspase-3 (**E**) in testicular organoids at 0–3 dpi. Nuclei were visualized with DAPI. Scale bar, 5 μm.

results revealed that though Leydig cells were not highly susceptible to ZIKV (Joguet et al., 2017), ZIKV infection still impaired testosterone synthesis of these cells. Our results also showed that ZIKV did not up-regulated the expression of apoptosis markers in testicular organoids, thus we believe that ZIKV infection was not the main factor leading to the damage of testicular cells.

5. Conclusions

In conclusion, our study provides an easily reproducible testicular organoid model that could mimic the pathological changes of ZIKV-infected testes. This model is a potentially powerful tool to investigate the role of different factors in ZIKV-induced testicular damage.

Data availability

All the data generated during the current study are included in the manuscript.

Ethics statement

All animal experiments were conducted in reviewed and approved by the Institutional Animal Care and the Animal Ethics Committees of Capital Medical University (Approval number: AEEI-2015-049).

Author contributions

Wei Yang: conceptualization, formal Analysis, investigation, writing-original draft, writing-review and editing. Chen Zhang: data curation, methodology, writing-original draft. Yan-Hua Wu: data curation, methodology. Li-Bo Liu: methodology, visualization. Zi-Da Zhen: data curation, methodology. Dong-Ying Fan: methodology, formal Analysis. Zheng-Ran Song: methodology. Jia-Tong Chang: methodology. Pei-Gang Wang: conceptualization, funding acquisition, resources, supervision, writing-review and editing. Jing An: conceptualization, funding acquisition, resources, supervision, writing-review and editing.

Conflict of interest

The authors declare that they have no conflict of interest.

Acknowledgements

This work was funded by the National Key Research and Development Plan of China (2021YFC2300202), the National Natural Science Foundation of China (U1902210, 81871641, 81972979, 82172266, 81902048), the Support Project of High-level Teachers in Beijing Municipal Universities in the Period of 13th Five-year Plan (IDHT20190510), and the Beijing Key Laboratory of Emerging Infectious Diseases (NO.DTKF202103). The funders had no role in study design, data collection and analysis, decision to publish, or preparation of the manuscript.

References

Cao-Lormeau, V.M., Blake, A., Mons, S., Lastere, S., Roche, C., Vanhomwegen, J., Dub, T., Baudouin, L., Teissier, A., Larre, P., Vial, A.L., Decam, C., Choumet, V., Halstead, S.K., Willison, H.J., Musset, L., Manuguerra, J.C., Despres, P., Fournier, E., Mallet, H.P., Musso, D., Fontanet, A., Neil, J., Ghawche, F., 2016. Guillain-Barre Syndrome

outbreak associated with Zika virus infection in French Polynesia: a case-control study. Lancet 387, 1531–1539.
Clevers, H., 2016. Modeling development and disease with organoids. Cell 165, 1586–1597.
Coffey, L.L., Pesavento, P.A., Keesler, R.I., Singapuri, A., Watanabe, J., Watanabe, R., Yee, J., Bliss-Moreau, E., Cruzen, C., Christe, K.L., Reader, J.R., von Morgenland, W., Gibbons, A.M., Allen, A.M., Linnen, J., Gao, K., Delwart, E., Simmons, G., Stone, M., Lanteri, M., Bakkour, S., Busch, M., Morrison, J., Van Rompay, K.K., 2017. Zika virus tissue and blood compartmentalization in acute infection of rhesus macaques. PLoS One 12, e0171148.
Driehuis, E., Kretzschmar, K., Clevers, H., 2020a. Establishment of patient-derived cancer organoids for drug-screening applications. Nat. Protoc. 15, 3380–3409.
Driehuis, E., Kretzschmar, K., Clevers, H., 2020b. Establishment of patient-derived cancer organoids for drug-screening applications. Nat. Protoc. 15, 3380–3409.
Dudley, D.M., Aliota, M.T., Mohr, E.L., Weiler, A.M., Lehrer-Brey, G., Weisgrau, K.L., Mohns, M.S., Breitbach, M.E., Rasheed, M.N., Newman, C.M., Gellerup, D.D., Moncla, L.H., Post, J., Schultz-Darken, N., Schotzko, M.L., Hayes, J.M., Eudailey, J.A., Moody, M.A., Permar, S.R., O'Connor, S.L., Rakasz, E.G., Simmons, H.A., Capuano, S., Golos, T.G., Osorio, J.E., Friedrich, T.C., O'Connor, D.H., 2016. A rhesus macaque model of Asian-lineage Zika virus infection. Nat. Commun. 7, 12204.
Dym, M., 1994. Basement membrane regulation of Sertoli cells. Endocr. Rev. 15, 102–115.
Ettayebi, K., Crawford, S.E., Murakami, K., Broughman, J.R., Karandikar, U., Tenge, V.R., Neill, F.H., Blutt, S.E., Zeng, X.L., Qu, L., Kou, B., Opekun, A.R., Burrin, D., Graham, D.Y., Ramani, S., Atmar, R.L., Estes, M.K., 2016. Replication of human noroviruses in stem cell-derived human enteroids. Science 353, 1387–1393.
Faizan, M.I., Abdullah, M., Ali, S., Naqvi, I.H., Ahmed, A., Parveen, S., 2016. Zika virus-induced microcephaly and its possible molecular mechanism. Intervirology 59, 152–158.
Ferraris, P., Yssel, H., Misse, D., 2019. Zika virus infection: an update. Microb. Infect. 21, 353–360.
Foy, B.D., Kobylinski, K.C., Chilson, F.J., Blitvich, B.J., Travassos, D.R.A., Haddow, A.D., Lanciotti, R.S., Tesh, R.B., 2011. Probable non-vector-borne transmission of Zika virus, Colorado, USA. Emerg. Infect. Dis. 17, 880–882.
Gagliano-Juca, T., Basaria, S., 2019. Testosterone replacement therapy and cardiovascular risk. Nat. Rev. Cardiol. 16, 555–574.
Garcez, P.P., Loiola, E.C., Madeiro, D.C.R., Higa, L.M., Trindade, P., Delvecchio, R., Nascimento, J.M., Brindeiro, R., Tanuri, A., Rehen, S.K., 2016. Zika virus impairs growth in human neurospheres and brain organoids. Science 352, 816–818.
Gassei, K., Schlatt, S., Ehmcke, J., 2006. De novo morphogenesis of seminiferous tubules from dissociated immature rat testicular cells in xenografts. J. Androl. 27, 611–618.
Gorman, M.J., Caine, E.A., Zaitsev, K., Begley, M.C., Weger-Lucarelli, J., Uccellini, M.B., Tripathi, S., Morrison, J., Yount, B.L., Dinnon, K.R., Ruckert, C., Young, M.C., Zhu, Z., Robertson, S.J., McNally, K.L., Ye, J., Cao, B., Mysorekar, I.U., Ebel, G.D., Baric, R.S., Best, S.M., Artyomov, M.N., Garcia-Sastre, A., Diamond, M.S., 2018. An immunocompetent mouse model of zika virus infection. Cell Host Microbe 23, 672–685 e6.
Govero, J., Esakky, P., Scheaffer, S.M., Fernandez, E., Drury, A., Platt, D.J., Gorman, M.J., Richner, J.M., Caine, E.A., Salazar, V., Moley, K.H., Diamond, M.S., 2016. Zika virus infection damages the testes in mice. Nature 540, 438–442.
Gyawali, N., Bradbury, R.S., Taylor-Robinson, A.W., 2016. The global spread of Zika virus: is public and media concern justified in regions currently unaffected? Infect Dis Poverty 5, 37.
Haddow, A.D., Nalca, A., Rossi, F.D., Miller, L.J., Wiley, M.R., Perez-Sautu, U., Washington, S.C., Norris, S.L., Wollen-Roberts, S.E., Shamblin, J.D., Kimmel, A.E., Bloomfield, H.A., Valdez, S.M., Sprague, T.R., Principe, L.M., Bellanca, S.A., Cinkovich, S.S., Lugo-Roman, L., Cazares, L.H., Pratt, W.D., Palacios, G.F., Bavari, S., Pitt, M.L., Nasar, F., 2017. High infection rates for adult macaques after intravaginal or intrarectal inoculation with zika virus. Emerg. Infect. Dis. 23, 1274–1281.
Hadley, M.A., Byers, S.W., Suarez-Quian, C.A., Kleinman, H.K., Dym, M., 1985. Extracellular matrix regulates Sertoli cell differentiation, testicular cord formation, and germ cell development in vitro. J. Cell Biol. 101, 1511–1522.
Halabi, J., Jagger, B.W., Salazar, V., Winkler, E.S., White, J.P., Humphrey, P.A., Hirsch, A.J., Streblow, D.N., Diamond, M.S., Moley, K., 2020. Zika virus causes acute and chronic prostatitis in mice and macaques. J. Infect. Dis. 221, 1506–1517.
Hirsch, A.J., Smith, J.L., Haese, N.N., Broeckel, R.M., Parkins, C.J., Kreklywich, C., DeFilippis, V.R., Denton, M., Smith, P.P., Messer, W.B., Colgin, L.M., Ducore, R.M., Grigsby, P.L., Hennebold, J.D., Swanson, T., Legasse, A.W., Axthelm, M.K., MacAllister, R., Wiley, C.A., Nelson, J.A., Streblow, D.N., 2017. Zika Virus infection of rhesus macaques leads to viral persistence in multiple tissues. PLoS Pathog. 13, e1006219.
Joguet, G., Mansuy, J.M., Matusali, G., Hamdi, S., Walschaerts, M., Pavili, L., Guyomard, S., Prisant, N., Lamarre, P., Dejucq-Rainsford, N., Pasquier, C., Bujan, L., 2017. Effect of acute Zika virus infection on sperm and virus clearance in body fluids: a prospective observational study. Lancet Infect. Dis. 17, 1200–1208.
Kumar, A., Jovel, J., Lopez-Orozco, J., Limonta, D., Airo, A.M., Hou, S., Stryapunina, I., Fibke, C., Moore, R.B., Hobman, T.C., 2018. Human Sertoli cells support high levels of Zika virus replication and persistence. Sci. Rep. 8, 5477.
Kurscheidt, F.A., Mesquita, C., Damke, G., Damke, E., Carvalho, A., Suehiro, T.T., Teixeira, J., Da, S.V., Souza, R.P., Consolaro, M., 2019. Persistence and clinical relevance of Zika virus in the male genital tract. Nat. Rev. Urol. 16, 211–230.
Lancaster, M.A., Knoblich, J.A., 2014. Organogenesis in a dish: modeling development and disease using organoid technologies. Science 345, 1247125.
Legendre, A., Froment, P., Desmots, S., Lecomte, A., Habert, R., Lemazurier, E., 2010. An engineered 3D blood-testis barrier model for the assessment of reproductive toxicity potential. Biomaterials 31, 4492–4505.
Lessler, J., Chaisson, L.H., Kucirka, L.M., Bi, Q., Grantz, K., Salje, H., Carcelen, A.C., Ott, C.T., Sheffield, J.S., Ferguson, N.M., Cummings, D.A., Metcalf, C.J., Rodriguez-Barraquer, I., 2016. Assessing the global threat from Zika virus. Science 353, aaf8160.
Li, C., Xu, D., Ye, Q., Hong, S., Jiang, Y., Liu, X., Zhang, N., Shi, L., Qin, C.F., Xu, Z., 2016. Zika virus disrupts neural progenitor development and leads to microcephaly in mice. Cell Stem Cell 19, 120–126.
Li, X., Ma, W., Wong, G., Ma, S., Li, S., Bi, Y., Gao, G.F., 2018. A new threat to human reproduction system posed by Zika virus (ZIKV): from clinical investigations to experimental studies. Virus Res. 254, 10–14.
Liu, W., Han, R., Wu, H., Han, D., 2018. Viral threat to male fertility. Andrologia 50, e13140.
Ma, W., Li, S., Ma, S., Jia, L., Zhang, F., Zhang, Y., Zhang, J., Wong, G., Zhang, S., Lu, X., Liu, M., Yan, J., Li, W., Qin, C., Han, D., Qin, C., Wang, N., Li, X., Gao, G.F., 2016. Zika virus causes testis damage and leads to male infertility in mice. Cell 167, 1511–1524 e10.
Ma, W., Li, S., Ma, S., Jia, L., Zhang, F., Zhang, Y., Zhang, J., Wong, G., Zhang, S., Lu, X., Liu, M., Yan, J., Li, W., Qin, C., Han, D., Qin, C., Wang, N., Li, X., Gao, G.F., 2017. Zika virus causes testis damage and leads to male infertility in mice. Cell 168, 542.
Mackay, S., Booth, S.H., MacGowan, A., Smith, R.A., 1999. Ultrastructural studies demonstrate that epithelial polarity is established in cultured mouse pre-Sertoli cells by extracellular matrix components. J. Electron. Microsc. 48, 159–165.
Matusali, G., Houzet, L., Satie, A.P., Mahe, D., Aubry, F., Couderc, T., Frouard, J., Bourgeau, S., Bensalah, K., Lavoue, S., Joguet, G., Bujan, L., Cabie, A., Avelar, G., Lecuit, M., Le Tortorec, A., Dejucq-Rainsford, N., 2018. Zika virus infects human testicular tissue and germ cells. J. Clin. Invest. 128, 4697–4710.
Mincheva, M., Sandhowe-Klaverkamp, R., Wistuba, J., Redmann, K., Stukenborg, J.B., Kliesch, S., Schlatt, S., 2018. Reassembly of adult human testicular cells: can testis cord-like structures be created in vitro? Mol. Hum. Reprod. 24, 55–63.
Mlera, L., Bloom, M.E., 2019. Differential Zika Virus Infection of Testicular Cell Lines. Viruses 11, 42.
Osuna, C.E., Lim, S.Y., Deleage, C., Griffin, B.D., Stein, D., Schroeder, L.T., Omange, R.W., Best, K., Luo, M., Hraber, P.T., Andersen-Elyard, H., Ojeda, E.F., Huang, S., Vanlandingham, D.L., Higgs, S., Perelson, A.S., Estes, J.D., Safronetz, D., Lewis, M.G., Whitney, J.B., 2016. Zika viral dynamics and shedding in rhesus and cynomolgus macaques. Nat. Med. 22, 1448–1455.
Pardi, N., Hogan, M.J., Pelc, R.S., Muramatsu, H., Andersen, H., DeMaso, C.R., Dowd, K.A., Sutherland, L.L., Scearce, R.M., Parks, R., Wagner, W., Granados, A., Greenhouse, J., Walker, M., Willis, E., Yu, J.S., McGee, C.E., Sempowski, G.D., Mui, B.L., Tam, Y.K., Huang, Y.J., Vanlandingham, D., Holmes, V.M., Balachandran, H., Sahu, S., Lifton, M., Higgs, S., Hensley, S.E., Madden, T.D., Hope, M.J., Kariko, K., Santra, S., Graham, B.S., Lewis, M.G., Pierson, T.C., Haynes, B.F., Weissman, D., 2017. Zika virus protection by a single low-dose nucleoside-modified mRNA vaccination. Nature 543, 248–251.
Pielnaa, P., Al-Saadawe, M., Saro, A., Dama, M.F., Zhou, M., Huang, Y., Huang, J., Xia, Z., 2020. Zika virus-spread, epidemiology, genome, transmission cycle, clinical manifestation, associated challenges, vaccine and antiviral drug development. Virology 543, 34–42.
Pletnev, A.G., Maximova, O.A., Liu, G., Kenney, H., Nagata, B.M., Zagorodnyaya, T., Moore, I., Chumakov, K., Tsetsarkin, K.A., 2021. Epididymal epithelium propels early sexual transmission of Zika virus in the absence of interferon signaling. Nat. Commun. 12, 2469.
Qian, X., Nguyen, H.N., Song, M.M., Hadiono, C., Ogden, S.C., Hammack, C., Yao, B., Hamersky, G.R., Jacob, F., Zhong, C., Yoon, K.J., Jeang, W., Lin, L., Li, Y., Thakor, J., Berg, D.A., Zhang, C., Kang, E., Chickering, M., Nauen, D., Ho, C.Y., Wen, Z., Christian, K.M., Shi, P.Y., Maher, B.J., Wu, H., Jin, P., Tang, H., Song, H., Ming, G.L., 2016. Brain-region-specific organoids using mini-bioreactors for modeling ZIKV exposure. Cell 165, 1238–1254.
Richer, G., Baert, Y., Goossens, E., 2020. In-vitro spermatogenesis through testis modelling: toward the generation of testicular organoids. Andrology-Us 8, 879–891.
Richner, J.M., Himansu, S., Dowd, K.A., Butler, S.L., Salazar, V., Fox, J.M., Julander, J.G., Tang, W.W., Shresta, S., Pierson, T.C., Ciaramella, G., Diamond, M.S., 2017. Modified mRNA vaccines protect against zika virus infection. Cell 168, 1114–1125 e10.
Robinson, C.L., Chong, A., Ashbrook, A.W., Jeng, G., Jin, J., Chen, H., Tang, E.I., Martin, L.A., Kim, R.S., Kenyon, R.M., Do, E., Luna, J.M., Saeed, M., Zeltser, L., Ralph, H., Dudley, V.L., Goldstein, M., Rice, C.M., Cheng, C.Y., Seandel, M., Chen, S., 2018. Male germ cells support long-term propagation of Zika virus. Nat. Commun. 9, 2090.
Sakib, S., Uchida, A., Valenzuela-Leon, P., Yu, Y., Valli-Pulaski, H., Orwig, K., Ungrin, M., Dobrinski, I., 2019. Formation of organotypic testicular organoids in microwell culturedagger. Biol. Reprod. 100, 1648–1660.
Schlatt, S., de Kretser, D.M., Loveland, K.L., 1996. Discriminative analysis of rat Sertoli and peritubular cells and their proliferation in vitro: evidence for follicle-stimulating hormone-mediated contact inhibition of Sertoli cell mitosis. Biol. Reprod. 55, 227–235.
Shan, C., Xie, X., Shi, P.Y., 2018. Zika virus vaccine: progress and challenges. Cell Host Microbe 24, 12–17.
Sheng, Z.Y., Gao, N., Wang, Z.Y., Cui, X.Y., Zhou, D.S., Fan, D.Y., Chen, H., Wang, P.G., An, J., 2017. Sertoli cells are susceptible to ZIKV infection in mouse testis. Front. Cell. Infect. Microbiol. 7, 272.
Siemann, D.N., Strange, D.P., Maharaj, P.N., Shi, P.Y., Verma, S., 2017. Zika virus infects human Sertoli cells and modulates the integrity of the in vitro blood-testis barrier model. J. Virol. 91, e00623–17.
Siu, M.K., Cheng, C.Y., 2004. Dynamic cross-talk between cells and the extracellular matrix in the testis. Bioessays 26, 978–992.

Siu, M.K., Cheng, C.Y., 2008. Extracellular matrix and its role in spermatogenesis. Adv. Exp. Med. Biol. 636, 74–91.
Strange, D.P., Jiyarom, B., Pourhabibi, Z.N., Xie, X., Baker, C., Sadri-Ardekani, H., Shi, P.Y., Verma, S., 2019. Axl promotes zika virus entry and modulates the antiviral state of human Sertoli cells. mBio 10, e01372–19.
Torres, J.R., Martinez, N., Moros, Z., 2016. Microhematospermia in acute Zika virus infection. Int. J. Infect. Dis. 51, 127.
Tung, P.S., Fritz, I.B., 1984. Extracellular matrix promotes rat Sertoli cell histotypic expression in vitro. Biol. Reprod. 30, 213–229.
van der Wee, K., Hofmann, M.C., 1999. An in vitro tubule assay identifies HGF as a morphogen for the formation of seminiferous tubules in the postnatal mouse testis. Exp. Cell Res. 252, 175–185.
von Kopylow, K., Schulze, W., Salzbrunn, A., Schaks, M., Schafer, E., Roth, B., Schlatt, S., Spiess, A.N., 2018. Dynamics, ultrastructure and gene expression of human in vitro organized testis cells from testicular sperm extraction biopsies. Mol. Hum. Reprod. 24, 123–134.
Willerton, L., Smith, R.A., Russell, D., Mackay, S., 2004. Effects of FGF9 on embryonic Sertoli cell proliferation and testicular cord formation in the mouse. Int. J. Dev. Biol. 48, 637–643.
Xu, D., Li, C., Qin, C.F., Xu, Z., 2019. Update on the animal models and underlying mechanisms for ZIKV-induced microcephaly. Annu Rev Virol 6, 459–479.
Yang, W., Wu, Y.H., Liu, S.Q., Sheng, Z.Y., Zhen, Z.D., Gao, R.Q., Cui, X.Y., Fan, D.Y., Qin, Z.H., Zheng, A.H., Wang, P.G., An, J., 2020. S100A4+ macrophages facilitate zika virus invasion and persistence in the seminiferous tubules via interferon-gamma mediation. PLoS Pathog. 16, e1009019.
Yu, J., Liu, X., Ke, C., Wu, Q., Lu, W., Qin, Z., He, X., Liu, Y., Deng, J., Xu, S., Li, Y., Zhu, L., Wan, C., Zhang, Q., Xiao, W., Xie, Q., Zhang, B., Zhao, W., 2017. Effective suckling C57bl/6, Kunming, and BALB/c mouse models with remarkable neurological manifestation for zika virus infection. Viruses 9, 165.
Zhang, X., Wang, L., Zhang, X., Ren, L., Shi, W., Tian, Y., Zhu, J., Zhang, T., 2017. The use of KnockOut serum replacement (KSR) in three dimensional rat testicular cells co-culture model: an improved male reproductive toxicity testing system. Food Chem. Toxicol. 106, 487–495.
Zhou, J., Li, C., Sachs, N., Chiu, M.C., Wong, B.H., Chu, H., Poon, V.K., Wang, D., Zhao, X., Wen, L., Song, W., Yuan, S., Wong, K.K., Chan, J.F., To, K.K., Chen, H., Clevers, H., Yuen, K.Y., 2018. Differentiated human airway organoids to assess infectivity of emerging influenza virus. Proc. Natl. Acad. Sci. U. S. A. 115, 6822–6827.